# MULTI-CAMERA PANORAMIC IMAGING SYSTEM CALIBRATION

D. Jarron [1],*, D. Lichti [1], M. Shahbazi [1], R. Radovanovic [2]

[1] Dept. of Geomatic Engineering, University of Calgary, T2N 1N4 Calgary, Alberta, Canada - (dmjarron, ddlichti, mozhdeh.shahbazi)@ucalgary.ca
[2] McElhanney Geomatics Engineering Ltd., T2G 0Y4 Calgary, AB, Canada - rradovanovic@ mcelhanney.net

**Commission I, WG I/7**

**KEY WORDS:** Ladybug Camera, Mobile Mapping, Camera Calibration, Panoramic Imaging

**ABSTRACT:**

A mobile mapping system (MMS) is a three-dimensional reality capture system that collects georeferenced spatial data with integrated navigation and imaging sensors from a moving vehicle. Several imaging subsystems can be found on board an MMS, such as panoramic camera systems and LiDAR sensors. The data collected from a panoramic imaging system must be accurately georeferenced and the sensors must be rigorously calibrated to ensure accurate registration of images to the point clouds collected by the LiDAR sensors, and to ensure panoramic images are generated seamlessly. The panoramic imaging system studied in this work is the Ladybug5 (by FLIR Integrated Imaging Solutions), which is a spherical camera system comprised of six individual wide-angle cameras. Having accurate estimates of the interior and relative orientation parameters of these cameras is essential for integrating the camera system with other sensors in the MMS to generate georeferenced spatial data. However, field experience has shown that factory-provided calibrations may be insufficiently accurate for high-precision applications. An investigation of the geometric calibration of the Ladybug 5 system was conducted in a dedicated indoor calibration facility at the University of Calgary: an 11 m x 11 m x 4 m field comprising 291 signalized photogrammetry targets. Multiple free-network, self-calibrating bundle adjustments were performed using different sets of constraints to model several systematic error sources. Weighted constraints were included in the adjustment to enforce the stability of the six relative orientation parameters between image pairs, and separate colour channel adjustments were used to compensate for chromatic aberrations. The overall fit of observations to the calibration model as measured by the root mean square error of the image point residuals was at the level of 0.3-0.4 pixels. Mean object point precision was at the 0.3 mm level. Rectified and ortho-rectified panoramas were also generated to verify the calibrations precision and observe how adjustments with constraints effect panorama generation.

## 1. INTRODUCTION

### 1.1 Literature Review

The Ladybug5 multi-camera system (Figure 1) is used for mobile mapping applications such as point cloud colouration and remote inspection. The Ladybug5 has six cameras: five horizontal and one vertical facing. Each camera, as well as the relative positions and orientations of the cameras, must be properly calibrated to maximize the accuracy of derived measurements. Factory calibration parameters may change over time, demonstrating a need for post-manufacture calibration.


Figure 1. Ladybug5 multi-camera system mounted on a RIEGL VMX MMS (RIEGL, 2017)

Panoramas generated from the Ladybug in certain environments have discontinuities that can be observed (Figure 2). In many applications such as point coloration remote measurement and feature detection, panoramas are required to be registered to underlying point clouds. In such situations, it is very important that panorama artefacts are minimized.

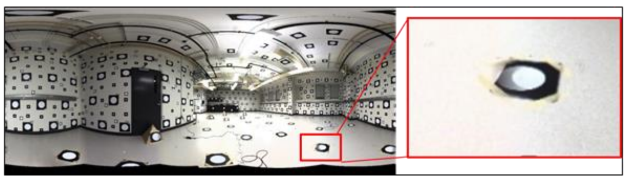

Figure 2. Example of stitch line discontinuities in Ladybug SDK generated panoramas

Calibration of Ladybug multi-camera systems has been reported by a few authors. Ikeda et al., (2003) calibrated a Ladybug system using a 2D calibration board and generated spherical panorama imagery by projecting onto a spherical surface at a large distance from the camera's centre of gravity (single projection point). The generated panoramas were found to stitch together with an average angular error of 0.3°. SIFT points extracted from imagery taken in a room of known size were used to perform a self-calibrating bundle adjustment of a Ladybug3 system (Schneider and Forstner, 2013). It was noted that the relative orientation parameters (ROP) angles differ by up to 0.6° from manufacturer specifications and ROP positions change by 1 – 4 mm. In Rau et al., (2016) calibration was performed with a coded target field to collect observations for a bundle adjustment. Separate calibration of the lenses and the relative orientation parameters (ROPs) was performed for using the camera system in a backpack MMS. Large amounts of uncompensated systematic error in cameras and cm-level object space errors were reported.

To the authors' best knowledge, Ladybug system calibration incorporating relative orientation stability constraints has not been reported. Calibrations using this methodology have been performed on other multi-camera systems. Single-step self-calibrating bundle adjustments utilizing ROP stability constraints have been reported for other multi-camera systems (Detchev et al., 2018; Lichti et al., 2015; Tommaselli et al., 2013). Single-step self-calibration is done by calibrating the interior orientation parameters (IOPs) of all cameras in the system while simultaneously estimating the exterior and relative orientation parameters and the object space reconstruction in a bundle adjustment. Tommaselli et al., (2013) shows that the single step self-calibration of multi-camera systems give lower image space observation residuals and object space root mean squared error (RMSE) than two step calibration, in which the cameras are pre-calibrated. Tommaselli et al., (2013) found that including ROP stability constraints increased image space observation residuals and object space RMSE, explained by the constraints keeping the EOPs from being correlated with intrinsic calibration parameters. The ROPs standard deviation is also decreased significantly by constraining the ROPs. In Lichti et al., (2015) and Tommaselli et al., (2013), the ROP stability is modelled using constraints as observations. Detchev et al., (2018) uses a model where the ROPs are considered as parameters that replace the exterior orientation parameters (EOPs) of the cameras. Only the reference camera's EOPs are determined and the rest are parameterized as relative transformations from the reference camera.

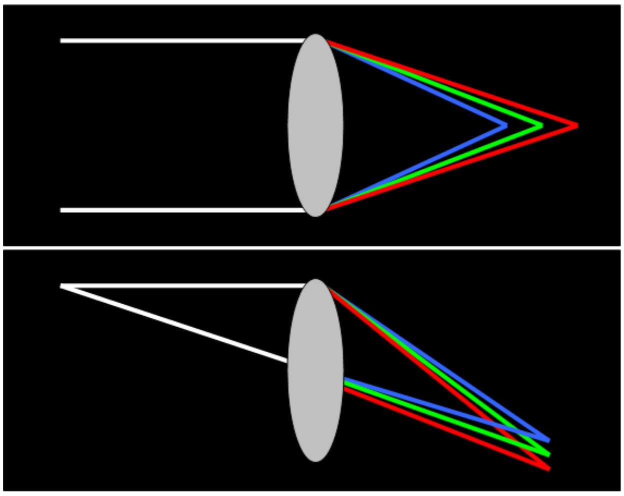

Figure 3 a) Top: Longitudinal chromatic aberration, b) Bottom: Lateral chromatic aberration.

Chromatic aberrations can also reduce the accuracy of a camera, and image quality. Chromatic aberrations occur in lateral and longitudinal forms due to wavelength-dependent refractions by the lens system (Figure 3). Longitudinal aberration causes each wavelength to have a different plane of best focus, and lateral aberrations cause lens distortions to be wavelength-dependent. The effect of lateral chromatic aberrations in Ladybug5 imagery can be seen in Figure 4. Modelling these errors in a self-calibrating bundle adjustment that separates the three channels of a true-colour image can improve image space observation residuals and object space RMSE (Luhmann et al., 2006). Luhmann et al. (2006) also found that wavelength-dependent radial lens distortion was caused by lateral chromatic aberrations which was also seen in Robson et al., 2014. Luhmann et al. (2006) also determined that positioning white targets is not affected by longitudinal chromatic aberrations.

Robson et al., (2014) calibrated a camera system with illumination from 21 different narrow light bands to determine correlations between wavelengths and different IOPs. The principal distance and the radial lens distortions varied strongly with wavelengths, and some variations were also seen with decentring, affinity, and shear distortions. In some cases, modelling the lateral and longitudinal aberrations do not entirely resolve the visible chromatic aberrations (Van Den Heuvel et al., 2006), at least in the case of fisheye cameras. In Luhmann et al. (2006), the EOPs of each of the three channels are constrained to be the same, and in Van Den Heuvel et al. (2006), each channel is modelled independently.

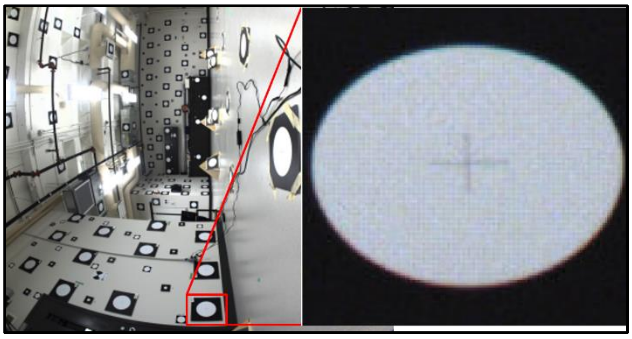

Figure 4. Longitudinal Chromatic Aberrations in Ladybug5 imagery.

### 1.2 Contributions

This paper provides a complete and rigorous calibration methodology for the Ladybug5 multi-camera panoramic imaging system. In this work, a single-step self-calibrating, free-network bundle adjustment is performed to find each camera's IOPs and lens distortion parameters, utilizing relative orientation stability constraints to enforce the reality of the camera's construction. This method also aims to resolve chromatic aberration by separating colour channels into three images and constraining EOPs between the three images within the bundle adjustment. Panoramas are generated using the estimated IOPs and ROPs to demonstrate the success of this calibration methodology.

## 2. METHODOLOGY

### 2.1 Collinearity Model

The camera is modelled as a pinhole camera using the augmented collinearity equations. It was determined that the radial lens distortions on the cameras were severe enough to warrant more parameters than the standard set. The model for radial lens distortion correction typically only extend to three parameters, but it was found that five are needed to accurately model observations at radial distances of greater than 1100 pixels. Equations 1 and 2 are the collinearity equations augmented with lens distortion parameters. Equation 3 describes the formation of the rotation matrix between object and image space using Euler angles. Equations 4-7 describe the different lens distortion parameters that are corrected. The parameters solved for are the IOPs $(x_p, y_p, c)$, the EOPs $(X_j^c, Y_j^c, Z_j^c, \omega, \phi, \kappa)$, and lens distortion parameters $(k_1, k_2, k_3, k_4, k_5, p_1 p_2)$.

$$x_{ij} = -c_j \frac{m_{11}(X_i-X_j^c)+m_{12}(Y_i-Y_j^c)+m_{13}(Z_i-Z_j^c)}{m_{31}(X_i-X_j^c)+m_{32}(Y_i-Y_j^c)+m_{33}(Z_i-Z_j^c)} + x_p + \Delta x_{ij} \quad (1)$$

$$y_{ij} = -c_j \frac{m_{11}(X_i-X_j^c)+m_{12}(Y_i-Y_j^c)+m_{13}(Z_i-Z_j^c)}{m_{31}(X_i-X_j^c)+m_{32}(Y_i-Y_j^c)+m_{33}(Z_i-Z_j^c)} + y_p + \Delta y_{ij} \quad (2)$$

$$\mathbf{M} = \mathbf{R_3}(\kappa)\mathbf{R_2}(\phi)\mathbf{R_1}(\omega) \quad (3)$$

$$\Delta x_{rad} = \bar{x}(k_1 r^2 + k_2 r^4 + k_3 r^6 + k_4 r^8 + k_5 r^{10}) \quad (4)$$

$$\Delta y_{rad} = \bar{y}(k_1 r^2 + k_2 r^4 + k_3 r^6 + k_4 r^8 + k_5 r^{10}) \quad (5)$$

$$\Delta x_{dec} = p_1(r^2 + 2\bar{x}^2) + 2p_2\bar{x}\bar{y} \quad (6)$$

$$\Delta y_{dec} = p_2(r^2 + 2\bar{y}^2) + 2p_1\bar{x}\bar{y} \quad (7)$$

$$\Delta x_{ij} = \Delta x_{rad} + \Delta x_{dec} \quad (8)$$

$$\Delta y_{ij} = \Delta y_{rad} + \Delta y_{dec} \quad (9)$$

where
$\mathbf{R_3}, \mathbf{R_2}, \mathbf{R_1}$ = the rotation sequence matrices
$\kappa, \phi, \omega$ = the Euler rotation angles between the object and image space
$\mathbf{M}$ = the rotation matrix
$x_p, y_p$ = the perspective centre of the camera in mm
$c_j$ = the principal distance of the camera in mm
$x_{ij}, y_{ij}$ = the image space coordinates of point i in image j in mm
$X_i, Y_i, Z_i$ = the object space coordinates of point i
$X_j^c, Y_j^c, Z_j^c$ = the object space coordinates of the perspective centre
$k_{1-5}$ = the radial lens distortion parameters
$p_1, p_2$ = the decentring lens distortion parameters
$\bar{x}$, $\bar{y}$ = the x and y distance from the perspective centre in mm
$\Delta x_{dec}, \Delta y_{dec}$= the decentring lens distortion correction
$\Delta x_{rad}, \Delta y_{rad}$= the radial lens distortion correction
$r$ = the distorted radial distance from the perspective centre of the image

## 2.2 ROP Stability Constraints

Each instance of the Ladybug's image capture creates six images, one from each camera. Each set of these six images should have approximately the same relative positions and angles between them. This assumes that the multi-camera system is stable during image capture, and that the ROPs of the cameras remain constant. Thus, a weighted constraint can be used to enforce the ROPs stability between image positions. Equation 10 describes the base vector between two cameras (left and right). Equation 11 describes the relative rotation matrix between the image spaces of the left and right image pair. Equations 12 and 13 show the constraints added based on the base vector and relative rotation angles. This enforces that the differences between ROP at different image pairs must be the same. The weighting refers to the relative contribution that the constraints will have to the adjustment.

$$\begin{pmatrix} b_X \\ b_Y \\ b_Z \end{pmatrix}_{LR} = \mathbf{M}_L \begin{pmatrix} X_R^c - X_L^c \\ Y_R^c - Y_L^c \\ Z_R^c - Z_L^c \end{pmatrix} \quad (10)$$

$$\Delta\mathbf{M}_{LR} = \mathbf{M}_{\mathrm{R}}\boldsymbol{M}_L^T = \mathbf{R}_3(\Delta\kappa_{LR})\mathbf{R}_2(\Delta\phi_{LR})\mathbf{R}_1(\Delta\omega_{LR}) \quad (11)$$

$$\begin{pmatrix} b_X \\ b_Y \\ b_Z \end{pmatrix}_{LR_1} - \begin{pmatrix} b_X \\ b_Y \\ b_Z \end{pmatrix}_{LR_2} = \begin{pmatrix} 0 \\ 0 \\ 0 \end{pmatrix} \quad (12)$$

$$\begin{pmatrix} \Delta\omega \\ \Delta\varphi \\ \Delta\kappa \end{pmatrix}_{LR_1} - \begin{pmatrix} \Delta\omega \\ \Delta\phi \\ \Delta\kappa \end{pmatrix}_{LR_2} = \begin{pmatrix} 0 \\ 0 \\ 0 \end{pmatrix} \quad (13)$$

where
$b_X, b_Y, b_Z$ = the base vector between the perspective centres of two cameras
$\Delta\kappa, \Delta\phi, \Delta\omega$ = the Euler rotation angles between the two cameras derived from $\Delta\mathbf{M}_{LR}$
$\mathbf{M}_{\mathrm{R}}$ = the rotation matrix from object to image space for the right camera in the pair
$\boldsymbol{M}_L^T$ = = the rotation matrix from image to object space for the left camera in the pair
$\Delta\mathbf{M}_{LR}$ = the rotation matrix between left and right camera in a camera pair

## 2.3 Chromatic Aberration Estimation

To estimate the lateral and longitudinal chromatic aberration, the imagery is separated into three channels: red (R), green (G), and blue (B). Image point observations are extracted from imagery of each three channels. To model the longitudinal aberration, each channel has is parameterized with its own principal distance. To model the wavelength-dependent lens distortion caused by lateral chromatic aberration, each channel has its own radial and decentring lens distortion parameters. In addition to the ROP stability constraints, new constraints are added to the EOPs of the three channels. The images derived from each channel of the same image, should have the same perspective centre. The position and angle elements of the three channels from the same image are constrained so that they are equal or similar to each other; see Figure 5. Without this, the images from separate channels have different orientations.

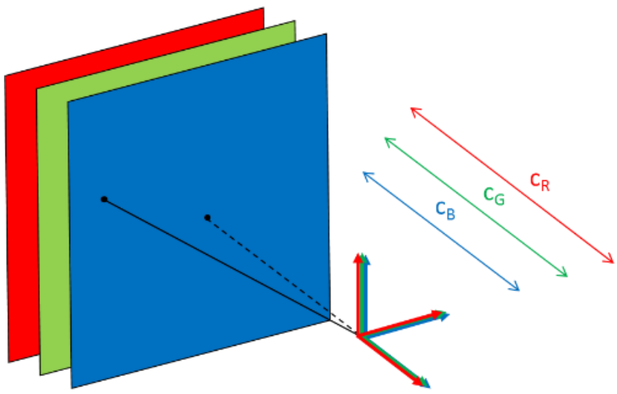


Figure 5. EOP constraints and variable principal distances for different colour channel imagery

## 2.4 Self-Calibrating bundle adjustment

The observations from all three channels are input to a bundle adjustment that simultaneously estimates the principal distances of each channel (red, green, blue) in each camera, along with lens distortions $(k_1, k_2, k_3, p_1, p_2, k_4, k_5)$ associated with each channel in each camera. This bundle adjustment also incorporates the ROP stability constraints to enforce the construction of camera across image pairs and the EOPs constraints between channels. Datum definition is performed by inner constraints (free network) imposed on the object points.

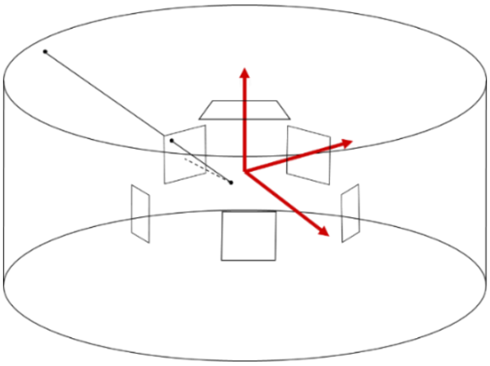

Figure 6. Ladybug Panorama projected onto cylinder

## 2.5 Cylindrical Panorama Generation

Using estimated parameters from the adjustment, panoramas can be generated and compared to imagery from the Ladybug software development kit (SDK). The SDK imagery shows significant discontinuities along stitches between images (Figure 2). There are multiple possible error sources to cause these discontinuities such as:

i. Projection centre disparity: where all images are projected from one approximated perspective centre, under the assumption that the true perspective centres are close enough together that they can be approximated by a single point (Ikeda et al., 2003). This is only true for images where objects are very far from the camera. This assumption is not true for all MMS environments, especially if close range objects like road signs, street lines, curbs, or powerlines are required to be surveyed.

ii. Uncompensated geometric errors or lens distortion: any uncompensated lens distortions may be accentuated in the projected panoramic image where the images overlap, as they will not fit together properly.

iii. Relief displacement: error due to large amounts of depth discontinuity between the projected surface and the object space

To correct these problems, the following steps are taken:

1. A canvas is generated in a size sufficient for imagery from the 5 horizontally oriented cameras. This can be visualized as an un-wrapped cylinder. Only the 5 horizontal cameras are used to generate panoramas in this work.
2. Each pixel in the canvas is projected onto the 3D model developed from the laser scan data (Figure 7).
3. Then, each of those object-space coordinates are back-projected into the space of each camera. This back-projected position is the rectified pixel position of the target.

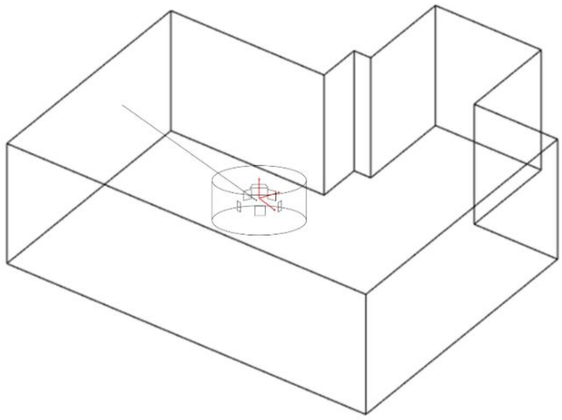

Figure 7. Geometric configuration for generation of Ladybug5 Orthorectified Panorama

To remove the effects of relief displacement, a 3D model of the object space was developed using laser scanning data. The model used in this experiment was rudimentary in construction, and a more detailed model would likely yield more accurate results in the future. Though a simple approximation of the calibration room, the model is sufficient to demonstrate the improvement as a result of the rigorous calibration and ortho-rectification. It is common in MMS to have integrated LiDAR and cameras on the same platform, which would allow for ortho-rectification of imagery captured of real-world environments. The five images are projected into the model of the object space, rather than a cylindrical or spherical approximation. Note that only geometric distortions were accounted for in the generation of the panorama. No photometric corrections such as alpha blending were considered at this time. In the future, the task of integrating the 6$^{th}$ camera (upward facing camera) will be performed.

## 3. EXPERIMENTS

Each of the Ladybug5's six cameras has a sensor size of 2448 x 2048, a pixel pitch of 0.00345 mm, and a nominal principal distance of 4.4 mm. Imagery from the Ladybug5 camera system was captured in a calibration room having controlled lighting and temperature. This room has dimensions approximately 11 m x 11 m x 4 m with 232 targets of 125 mm radius made from 4 mm thick BubbleX plastic, and 59 paper targets of 40 mm radius, which cover the walls, ceiling, and floor of the calibration space. Smaller targets also exist in the calibration space, but they are ignored in these experiments. Before data acquisition with the cameras was performed, the targets in the calibration space were imaged with a Faro Focus 3D laser scanner, and the centre coordinates of each target were extracted by fitting a circle to the edge points, as seen in Figure 8. (Lichti et al., In Press).

Many images were captured to perform the calibration, with 262 images being used from the six cameras. Images were taken from different heights and with orthogonal roll angles utilizing convergent geometry. Imagery in both landscape and portrait orientations were acquired. Images of the calibration space can be seen in Figures 2, 12, and 13. The images were taken in JPEG format to simulate image capture in a mobile mapping setting where buffering and speed are important factors.

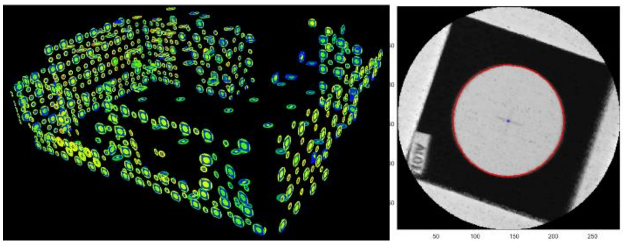

Figure 8. a) Left: Display of object space coordinate survey using laser scan data b) Right: close up of laser scanned targets centre being determined in the laser scan data

Automated target measurement was performed using the algorithm described by (Jarron et al., In Press). It is briefly summarized here. In each image, the circular targets were detected using adaptive thresholding and robust ellipse fitting. Labelling of the targets was performed next. First, the exterior orientation parameters of the image were estimated using a one-point pose-estimation approach, where a list of possible orientation and target labels was used, along with approximate camera height, to calculate the camera position. The estimated position and orientation of the camera combined with the interior orientation parameters (IOPs) were then used to back-project the known object-space coordinates of the targets into the image space. These targets were then matched against the targets detected in the image, and the list entry with the best fit is chosen as the solution

The panoramas were generated using the methodology described in Section 2.5. The cylindrical panoramas were made on a canvas of 10240 x 2448 pixels. Each pixel in the panorama was projected onto the surface of a 3D model. This model was developed using the same laser scanning data that the target data was extracted from. To ensure observed discontinuities were not caused by projection centre disparity or relief displacement, cylindrical and ortho-rectified cylindrical panoramas were generated from both the factory and the estimated parameters. Rectified and ortho-rectified panoramas were generated using both the estimated parameters and the factory parameters, both with and without the use of ROP stability constraints. These panoramas were used to verify the quality of the calibration procedure.

## 4. RESULTS

### 4.1 Calibration of Ladybug5 using different constraints

A series of different types of adjustments was performed and compared. The greyscale imagery is generated using the conversion defined in Equation 14. The three main adjustment types are the un-constrained adjustment using the greyscale imagery only (1986 unknowns, 10649 degrees of freedom), an adjustment with ROP stability constraints using greyscale imagery only (1986 unknowns, 11903 degrees of freedom), and an adjustment with both ROP stability constraints and EOP stability constraints using imagery broken into red, green, and blue images, with much higher weights for the ROP constraints (5250 unknowns, 40531 degrees of freedom).

$$Grey = 0.2125R + 0.7154G + 0.0721\,B \tag{14}$$

where $R, G, B$ = the colour intensity of the channel

Table 1. RMS of pixel space residuals, mean object space reconstruction precision ($\bar{\sigma}$), and RO stability of 3 adjustments: Unconstrained greyscale adjustment (A), Greyscale Adjustment with ROP stability constraints (B), RGB combined adjustment with ROP and EOP stability constraints (C)

| Adjustment Type | A | B | C |
|---|---|---|---|
| RMS x (pixels) | 0.25 | 0.26 | 0.39 |
| RMS y (pixels) | 0.29 | 0.33 | 0.45 |
| $\bar{\sigma}_X$ Object Space (mm) | 0.32 | 0.30 | 0.30 |
| $\bar{\sigma}_Y$ Object Space (mm) | 0.34 | 0.31 | 0.38 |
| $\bar{\sigma}_Z$ Object Space (mm) | 0.21 | 0.20 | 0.42 |
| RMS RO position (mm) | 4.92 | 0.43 | 0.001 |
| RMS RO angle(") | 227 | 15 | 0.036 |

The unconstrained adjustment has the lowest observation residuals of any adjustment. This is similar to results described in other works (Detchev et al., 2018; Lichti et al., 2015), where RMS values increase when ROP stability constraints are utilized. Constraining the ROPs enforces the structure of the camera, forcing error to propagate elsewhere in the network. Including the ROP stability constraints increases the object space reconstruction precision, as can be seen in Table 1 between the unconstrained and ROP stability constrained greyscale adjustments, A and B, respectively. This indicates that even though the observation residual RMS increases, the 3D reconstruction is slightly more precise. The RO values of adjustment A show that in an unconstrained adjustment the ROPs vary considerably. The adjustment that separated the RGB channels into separate images for the adjustment has higher RMS observation residuals and the worst object-space reconstruction precision. One reason for this may be that separating the channels into different imagery effectively cuts the amount of information in those images based on the Bayer pattern of the sensor, lowering the precision of target detection. Another likely reason is this adjustment has the most rigidly enforced constraints, forcing any errors out of the EOPs and elsewhere in the adjustment. Separating the channels into imagery allows for the compensation of chromatic aberrations but appears to influence the precision of the object space reconstruction negatively. This may mean that chromatic aberrations should only be corrected if their effect on the image quality is severe enough to warrant the resulting drop in precision. It remains to be tested how each of these adjustments' errors reflect on check points.

Figure 10 demonstrates how the principal distance varies across the red, green, and blue channels. In theory, blue should be the shortest, and red the longest. For cameras 3-5 this holds true, but not with cameras 0-2. For almost all cameras, each principal distance is within the 95% confidence interval of the other channels. The variance in the principal distances is relatively small in effect, compared to the large difference in the radial lens distortions indicated in Figure 10. This indicates that the lateral chromatic aberration has a larger effect than the longitudinal chromatic aberration on the image quality.

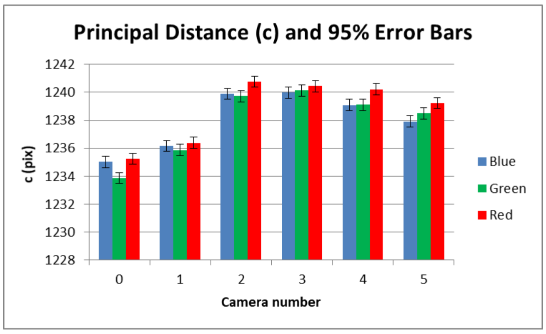


Figure 10. Principal distance in pixels with 95% error bars, variance across different channels

Modelling the radial distortion as being wavelength-dependent can improve the image quality at the edges of the images significantly. Figure 11b shows how large the differences between the red and green radial lens errors are at the edge of the image. The difference between them is close to 30 pixels, which would be easily visible. This error increases quickly, with the radial error at the radii of 1000 pixels only resulting in 1 pixel of difference between red and green channels. The difference in the corrections between the factory and estimated parameters can be seen in Figure 11c. This large difference indicated that near the edge of the image, the radial distortion is modelled differently, and the correction made are much different.

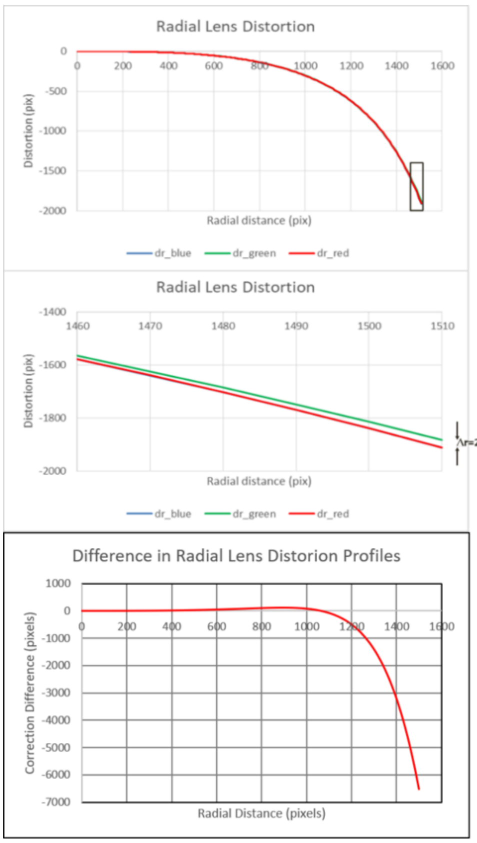


Figure 11. Radial lens distortion profile of Ladybug 5 camera 0, separate based on colour channel. a) Top: full distortion curve. b) Middle: expanded area of curve, from area highlighted with a black box in top graph. C) Bottom: Difference in radial distortion correction between factory and estimated parameters

Table 2. Difference in ROP base vectors between estimated (adjustment C) and factory parameters

| Cameras | | Factory - Estimated | | | Length |
|---|---|---|---|---|---|
| from | to | $b_X$ (mm) | $b_Y$ (mm) | $b_Z$ (mm) | $\|b\|$ (mm) |
| 0 | 1 | -0.1 | -1.4 | 1.3 | -0.4 |
| 0 | 2 | 0.1 | -3.3 | 0.9 | -0.2 |
| 0 | 3 | 0.2 | -4.1 | -1.3 | 0.0 |
| 0 | 4 | 0.0 | -1.7 | -1.8 | 0.3 |
| 0 | 5 | 0.4 | 1.3 | -0.3 | -0.5 |

The results in Table 2 are similar to those found in Schneider and Forstner, (2013) where it was found that RO position varies by 1-4 mm. Table 3 shows that the difference between the estimated ROP angles are very large, on average 0.2°. This is also quite similar to the results of Schneider and Forstner, (2013).

Table 3. Difference in ROP angles between estimated (adjustment C) and factory parameters

| Cameras | | Factory - Estimated | | |
|---|---|---|---|---|
| from | to | $\Delta\omega$ (°) | $\Delta\phi$ (°) | $\Delta\kappa$ (°) |
| 0 | 1 | 0.01 | 0.36 | 0.07 |
| 0 | 2 | 0.02 | 0.17 | -1.37 |
| 0 | 3 | 0.02 | -0.79 | -0.56 |
| 0 | 4 | 0.05 | -0.55 | -0.07 |
| 0 | 5 | 14.25 | -179.38 | -260.08 |

### 4.2 Comparison of Rectified Panoramas generated with estimated parameters and factory parameters

To examine the need for post-factory calibration of devices such as the Ladybug5, the factory-derived parameters were used to generate panoramas, and these are compared to the panoramas generated from the newly estimated parameters from the RGB separated channel adjustment. Both cylindrical projection panoramas show significant discontinuities (Figures 12a and 12b). The panorama generated using the factory parameters has large errors due to uncompensated lens distortion, while the panorama generated using the estimated parameters does not.

### 4.3 Comparison of Ortho-rectified Panoramas generated with estimated parameters and factory parameters

The ortho-rectified panorama using the newly estimated parameters shows a significant improvement, with most discontinuities being reduced to a few pixels (Figure 13b). However, the ortho-rectified panorama generated using the factory parameters (Figure 13a) still shows significant distortions and discontinuities. This demonstrates that the factory parameters are no longer valid for the camera that was tested in this experiment, and that new parameters may need to be determined periodically. It is also worth noting that the factory calibration parameters only use 4 parameters for radial lens calibration, in comparison to the 5 used in estimated parameters. Determining the stability of the camera system in

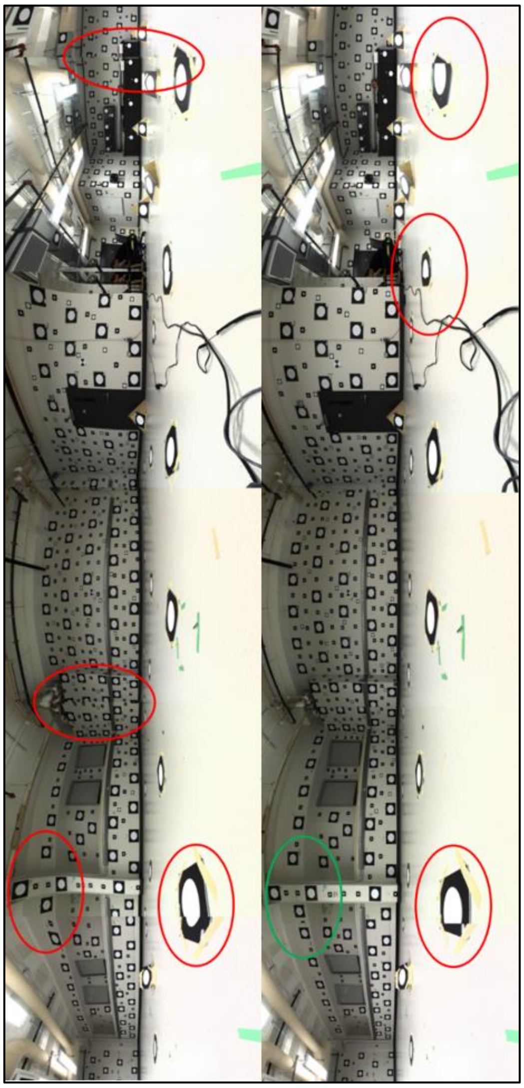

Figure 12. Rectified Image panoramas with 5 horizontal images a) Left: Using factory IOPs and ROPs projected onto a cylinder. b) Right: Using newly estimated IOPs and ROPs projected onto a cylinder. Areas of extreme discontinuity or uncompensated lens distortion circled in red. Green circle shows area of improvement over factory parameters

the future could provide insight into how often calibration is necessary. For the Ladybug5 system, ortho-rectification seems to be necessary for the generation of a reasonably accurate panorama with no discontinuities along the stitch lines between its component images.

### 4.4 Effect of ROP constraints using different panoramas

A more qualitative method for evaluating each adjustment is examining their resulting panoramas. As can be seen in Figures 14 and 15, in adjustments without imposed ROP stability constraints, there is an angular discontinuity along the seam lines of the panorama. Imposing ROP constraints seems to reduce these discontinuities. This implies that the ROP constraints positively affect the 3D reconstruction and panorama generation of the camera.

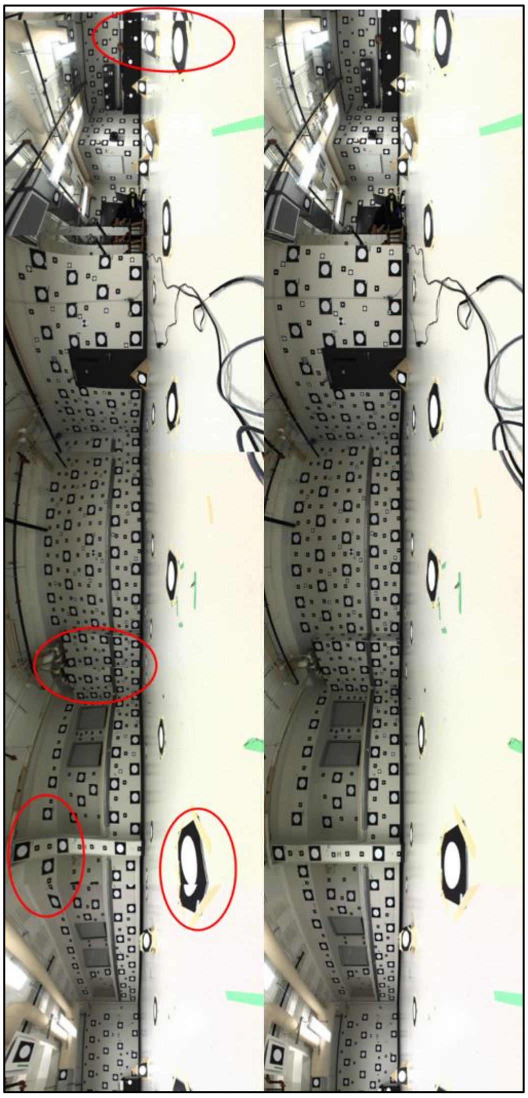

Figure 13. Ortho-rectified image panoramas with 5 horizontal images a) Left: Using factory IOPs and ROPs. b) Right: Using newly estimated IOPs and ROPs. Areas of extreme discontinuity or distortion circled in red.

## 5. CONCLUSION

In this work, a complete methodology has been developed for the calibration and accurate panorama generation for the Ladybug5 multi-camera system. Using ROP stability constraints and separating the colour channels into separate images, a more accurate calibration can be performed, generating sub millimetre object space reconstruction precision and image space observation residuals in the range of 0.3-0.4 pixels. Combining this new adjustment with ortho-rectification techniques, a more accurate panorama has been produced. This panorama will be more effective for site inspection and other common uses of panoramic imagery in mobile mapping. A comparison of these results and those generated using the factory calibration parameters show that the newly generated results outperform the factory calibration in the quality of generated panoramas. The panoramas generated by the factory calibration, even when ortho-rectified, showed significant distortions and discontinuities along the stitch lines. Integrating the sixth camera into the panorama generation still needs to be completed

The stability of the camera remains to be determined. The factory parameters for the camera used in this work were no longer effective. Temporal stability analysis could be performed to determine how often calibration should be done. It would also determine how reasonable it is to constrain the ROPs. If the ROPs change regularly, using ROP stability constraints in the calibration may not be a worthwhile technique.

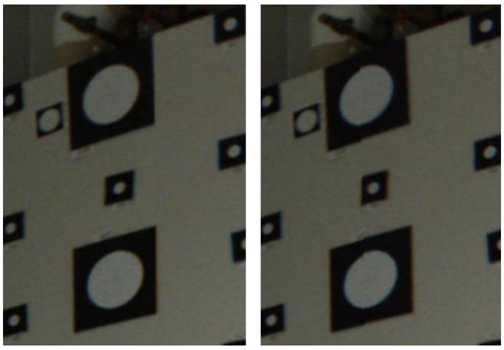

Figure 14. Close up of a stitch line of generated panoramas. a) Panorama generated from adjustment using ROP stability constraints. b) Panorama generated from adjustment without stability constraints

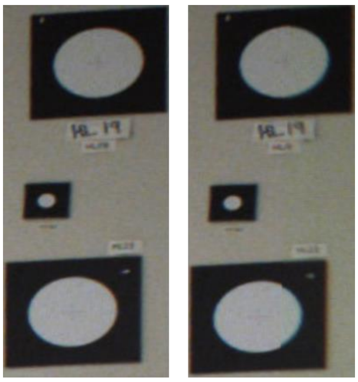

Figure 15. Another Close up of a stitch line of generated panoramas. a) Panorama generated from adjustment using ROP stability constraints. b) Panorama generated from adjustment without stability constraints

In addition, utilizing the collinearity model for this camera may not be the optimal approach. Using five radial lens distortion parameters results in very high correlations between the parameters and may be overfitting the observations. Future work will consider alternate models, such as a fisheye lens model, for modelling the Ladybug5 and other similar wide-angle lens cameras.

## 6. REFERENCES


Detchev, I., Habib, A., Mazaheri, M., Lichti, D., 2018. Practical In Situ Implementation of a Multicamera Multisystem Calibration. Journal of Sensors 2018, 1–12. https://doi.org/10.1155/2018/5351863

Ikeda, S., Sato, T., Yokoya, N., 2003. High-resolution panoramic movie generation from video streams acquired by an omnidirectional multi-camera system, in: Presented at *the Proceedings of IEEE International Conference on Multisensor Fusion and Integration for Intelligent Systems,* MFI2003., pp. 155–160. https://doi.org/10.1109/MFI-2003.2003.1232649

Jarron, D., Shahbazi, M., Lichti, D., Radovanovic, R., (In Press). Automatic Detection and Labelling Of Photogrammetric Control Points In A Calibration Test Field, in: *ISPRS Annals of the Photogrammetry, Remote Sensing and Spatial Information Sciences*. Presented at the ISPRS Geospatial Week 2019, University of Twente, Enschede, Netherlands, p. 8.

Lichti, D., Jahraus, A., Hartzell, P., (In Press) New approach for low-cost TLS target measurement. ASCE *Journal of Surveying Engineering* Accepted 13/02/2019.

Lichti, D.D., Sharma, G.B., Kuntze, G., Mund, B., Beveridge, J.E., Ronsky, J.L., 2015. Rigorous Geometric Self-Calibrating Bundle Adjustment for a Dual Fluoroscopic Imaging System. *IEEE Transactions on Medical Imaging* 34, 589–598. https://doi.org/10.1109/TMI.2014.2362993

Luhmann, T., Hastedt, H., Tecklenburg, W., 2006. MODELLING OF CHROMATIC ABERRATION FOR HIGH PRECISION PHOTOGRAMMETRY. *ISPRS - International Archives of the Photogrammetry, Remote Sensing and Spatial Information Sciences XXXVI*, 6.

Rau, J.Y., Su, B.W., Hsiao, K.W., Jhan, J.P., 2016. Systematic Calibration For A Backpacked Spherical Photogrammetry Imaging System. *ISPRS - International Archives of the Photogrammetry, Remote Sensing and Spatial Information Sciences XLI*-B1,695–702.https://doi.org/10.5194/ isprsarchives-XLI-B1-695-2016

RIEGL, 2017. Caltrans Takes Delivery of the RIEGL VMX-1HA. The RIEGL Newsroom. URL https://newsroom.riegl.international/2017/01/11/caltrans-takes-delivery-of-the-riegl-vmx-1ha/ (accessed 2.19.19).

Robson, S., MacDonald, L., Kyle, S.A., Shortis, M.R., 2014. Multispectral calibration to enhance the metrology performance of C-mount camera systems. *ISPRS - International Archives of the Photogrammetry, Remote Sensing and Spatial Information Sciences XL*–5, 517–521. https://doi.org/10.5194/isprsarchives-XL-5-517-2014

Schneider, J., Forstner, W., 2013. Bundle Adjustment and System Calibration with Points at Infinity for Omnidirectional Cameras. Institute of Geodesy and Geoinformation, University of Bonn, Germany.

Tommaselli, A., Galo, M., de Moraes, M., Marcato, J., Caldeira, C., Lopes, R., 2013. Generating Virtual Images from Oblique Frames. *Remote Sensing* 5, 1875–1893. https://doi.org/10.3390/rs5041875

Van Den Heuvel, F.A., Verwaal, R., Beers, B., 2006. Calibration of fisheye camera systems and the reduction of chromatic aberration, in: Proceedings ISPRS Commission V Symposium, *IAPRS Vol. XXXVI*, Part 5.